Sensors and Materials, Vol. 35, No. 8 (2023) 3045–3055
MYU Tokyo

S & M 3373

Using Autoencoder Artificial Neural Network to Predict Photonic Crystal Band Structure

Wei-Shan Chang,[1] Ying-Pin Tsai,[2] Chi-Tsung Chiang,[1] and Fu-Li Hsiao[1*]

[1]Institute of Photonics, National Changhua University of Education
No. 1, Jin-De Road, Changhua City 50007, Taiwan
[2]College of Photonics, National Yang Ming Chiao Tung University
Chi-Mei Building, No. 301, Sec. 2, Gaofa 3rd Rd., Guiren Dist., Tainan City 71150, Taiwan

(Received December 30, 2022; accepted July 12, 2023)

Keywords: photonic band structures, encoders, neural networks

A photonic crystal is an artificial material with a periodic optical refractive index. The band structure of photons can be tailored by adjusting the geometric parameters spatially. By properly designing the configuration, the photonic crystal can generate an optical forbidden band within the structure. To choose an appropriate geometric configuration that can generate a photonic band gap in the desired frequency range, traditionally, the band structure of such structure has been obtained by applying Floquet periodic boundary conditions and performing the eigen analysis calculation. However, a great amount of testing is required and consumes a great amount of time. In our study, the top view of the unit cell is converted to a binary bitmap and encoded to downgrade the bitmap for forming the input data of the artificial neural network. We adopted the finite element method to calculate the band structure training data set, which contained various geometric parameters and corresponding band structures. Our neural network shows high accuracy and is less time-consuming. The results are useful for the inverse design of photonic crystals.

1. Introduction

A photonic crystal is an artificial material. The spatial distribution of the refractive index of the photonic crystal is periodic. The concept of the photonic crystal was inspired by the energy band diagram of semiconductors in solid-state physics. The electron wave in a semiconductor experiences spatially periodic potential. The dispersion relation of the electron wave can be tailored by adjusting the periodic potential.(1,2) The periodic potential generates a certain energy gap. The electron cannot exist in a semiconductor when the energy of this electron is within the energy gap. A concept similar to the use of a energy gap of the electron wave has been applied to the optical wave. Originally, the spatially periodic refractive index structure was proposed to suppress the spontaneous emission of laser systems. Many phenomena such as slow light, ultrasmall optical cavity, negative refraction, and topological photonic crystals have been

*Corresponding author: e-mail: fulihsiao@cc.ncue.edu.tw
https://doi.org/10.18494/SAM4514

ISSN 0914-4935

investigated.[3–6] The applications of photonic crystal devices are also diverse. The photonic crystal structure can be used in optical communication, optical filtration, and sensing.[7–9]

The periodicity of a photonic crystal can be one-, two- or three-dimensional. In recent years, photonic crystals based on strip or slab waveguides with periodic structures have also been attracting much attention. Most photonic crystals consist of two materials with different refractive indexes. The geometric configuration and refractive index contrast between the two materials directly govern the dispersion relation of photonic crystals. The dispersion relation of photonic crystals is usually represented by the photonic band structure. The band structure indicates the relationship between the optical angular frequency and the wave vectors. Because the photonic crystals are spatially periodic, the wave vector within the Brillouin zone can represent all directions of the structure. By properly manipulating the geometric configuration and refractive index contrast of the photonic crystal, the optical forbidden frequency gap can be opened or a low group velocity can be achieved. In addition, the negative refraction or topological photonic phenomenon can be achieved by tailoring the photonic band structure. By introducing certain defects of spatial periodicity into the photonic crystal, we can create optical cavities or waveguides to trap the optical energy. The optical cavities and waveguides of photonic crystals can confine the optical energy in the sub-wavelength region and thus enable their use in many novel applications.[10,11]

The features of photonic crystals are mostly based on the photonic band structure. The photonic crystal band structure can be obtained by solving the eigen frequencies of a unit cell under specific periodic boundary conditions. There are several numeric tools that can be used for the calculation of the photonic crystal band structure, such as the plane wave expansion and finite element methods.[12,13] Although the photonic crystal band structure is strongly related to the geometric configuration and refractive index distribution of photonic crystals, the relationships among them are not intuitive. The change in band structure depending on the geometric parameters and refractive index distribution is complex and nonlinear. Therefore, huge numbers of combinations should be examined to obtain the desired band structure. On the other hand, the numeric tools for calculating the photonic crystal band structure are usually time-consuming. Therefore, it takes a great amount of time to obtain a desired photonic crystal band structure.

In recent years, deep learning has attracted much attention in various fields of research and application. Deep learning and artificial neural networks are powerful tools for dealing with complex and nonlinear problems.[14–17] They are also applied to the research of electromagnetic waves, such as those in optical gratings, optical ring resonator sensors, and photonic crystals.[18–21] For example, artificial neural networks are used to predict the diffractive efficiencies of optical gratings.[18] The diffractive efficiencies of each order of an optical grating are strongly related to the geometric shape of the grating. The relationship between the diffractive efficiency and geometric shape of an optical grating is complex and nonlinear. The change the diffractive efficiency depending on the geometric parameters has been calculated and used to train artificial neural networks.[18] A well-trained artificial neural network can predict the diffractive efficiency using the given geometric parameters. Its prediction time is much shorter than those of traditional numeric calculations. The artificial neural networks are

also effective for solving inverse design problems. In a traditional design process, researchers must modify the geometric shape of the grating repeatedly in order to obtain the desired results. In the application of an artificial neural network, the diffractive efficiencies and geometric parameters of the grating can be considered as input and output data, respectively. Through proper training, the artificial neural network can generate suitable geometric parameters of a grating in accordance with the desired diffractive efficiency.

In this study, we aim to train artificial neural networks to predict the two-dimensional photonic crystal band structure. The training data are generated by finite element simulation, which is extensively used in photonic crystal research. First, the proposed artificial neural networks can identify the image of a unit cell of the photonic crystal structure through the use of an autoencoder. The autoencoder is trained in an unsupervised fashion. Second, the artificial neural networks can predict the eigen frequency of a specific photonic band from the unit cell image information, given the wave vector in a reciprocal lattice and the band order. We test two neural network configurations with different numbers of hidden layers. The predicted results agree well with the results calculated by the finite element method.

2. Photonic Crystal Structures and Artificial Neural Network Configuration

In this study, we focus on the two-dimensional square lattice silicon photonic crystal structure. The photonic crystal consists of a square lattice of an air cylinder array in the silicon host. Figure 1(a) shows a schematic of the top view of the unit cell of a two-dimensional square

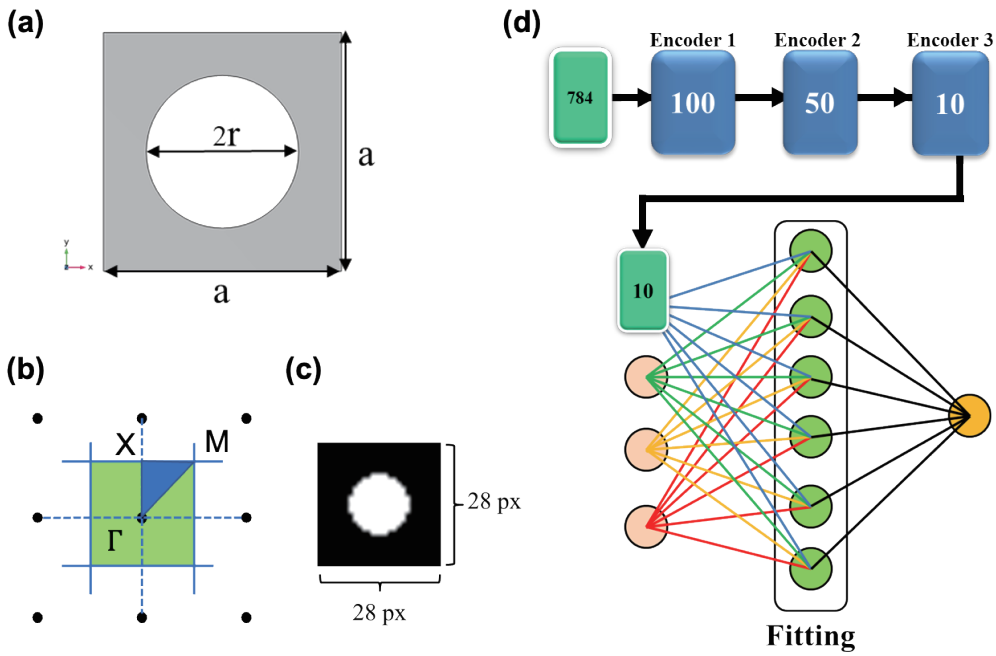

Fig. 1. (Color online) (a) Top view of unit cell of two-dimensional photonic crystal. (b) Reciprocal lattice of square lattice. (c) Binary bitmap converted from the top view of unit cell. (d) Schematic of artificial neural network.

lattice silicon photonic crystal. The gray area is silicon and the white circle is the air cylinder. The lattice constant is denoted by "a". The radius of the air cylinder is denoted by "r". Figure 1(b) represents the reciprocal lattice of the square lattice.[22] The vectors in the reciprocal lattice are wave vectors and are denoted by "k". The green area in the reciprocal lattice is the first Brillouin zone. The blue triangle is the irreducible Brillouin zone, which is the first Brillouin zone reduced by all of the symmetries in all directions. Then, the wave dispersion behaviors in the periodic structure can be represented by the dispersion relation within the irreducible Brillouin zone.

The photonic band structure calculation based on the finite element method yields the eigen state and eigen frequency of an optical wave in a unit cell with the Floquet periodic boundary condition. The Floquet periodic boundary condition depends on the wave vector in the irreducible Brillouin zone. The wave vectors $\vec{k}$ in the irreducible Brillouin zone start from the Γ point. The end points of $\vec{k}$ sweep from the Γ point to the X point, then turn toward the M point and return to the Γ point. We denote the wave vector as $\vec{k} = k_x\hat{x} + k_y\hat{y}$. For the eigen frequency calculation of a certain $\vec{k}$ vector, the periodic boundary condition with a k_x phase difference is applied between the x boundaries of the unit cell, and the periodic boundary condition with a k_y phase difference is applied between the y boundaries of the unit cell. The photonic band structure can be obtained by sweeping the end points of $\vec{k}$ step by step and repeating the eigen state analysis by the finite element method. One calculation result is illustrated in Fig. 2(a). The blue circles represent the eigen frequencies calculated by the finite element method (COMSOL

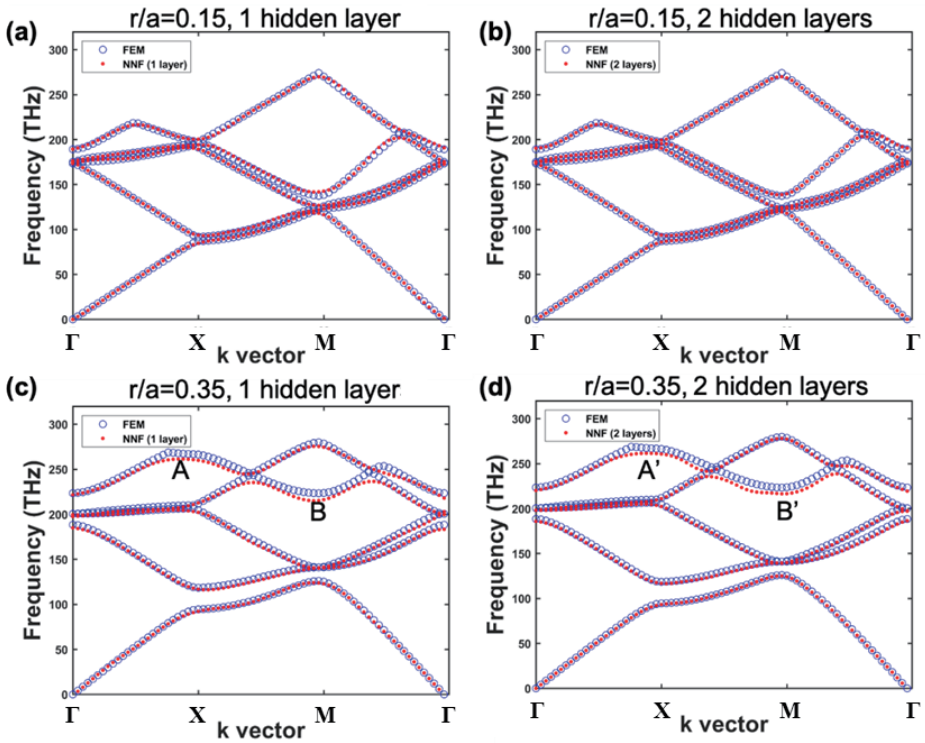

Fig. 2. (Color online) Band structures calculated by finite element method (blue circles) and predicted by trained neural network (red dots). The r/a ratios of the structure are 1.5 in (a), (b) and 0.35 in (c), (d). The numbers of hidden layers in the neural network are one in (a), (c) and two in (b), (d).

Multiphysics). The horizontal axis denotes the end points of $\vec{k}$ vectors. The edge of the irreducible Brillouin zone is divided into 75 steps, i.e., we performed the eigen analysis 75 times to obtain the band structure in Fig. 2(a). For each $\vec{k}$ vector, we calculated five orders of eigen frequencies.

Figure 1(c) shows the binary bitmap converted from the top view of the unit cell. The r/a ratio is 0.25. The bitmap is 28 × 28 pixels. In this study, we use the neural network toolbox of commercial software (MATLAB) to construct the artificial neural network. The configuration of the neural network is illustrated in Fig. 1(d). First, we use three unsupervised trained autoencoders to reduce the size and extract the features of the bitmap. Second, the extracted features of the unit cell are combined with the $\vec{k}$ vector and orders of eigen frequencies to form the input data, and the eigen frequencies calculated by the finite element method are the output data. We use the input and output data to train a fitting neural network to predict the eigen frequencies.

The compression of bitmaps is illustrated at the top of Fig. 1(d). The task of the autoencoder is to compress the information of the input image while retaining the features of the image. Therefore, the outputs of each autoencoder are less than their inputs. The unsupervised training of the autoencoder is as follows. An image is input to an encoder and the dimension is reduced to a customized output. A decoder is connected behind the encoder, and the original image is reconstructed from the output of the encoder. Because the photonic crystal is composed of only two materials, the geometric configuration can simultaneously represent the distribution of refractive indexes. The input bitmap of the unit cell contains 784 pixels (28 × 28). The first trained encoder compresses the original bitmap to 100 outputs. The second trained encoder compresses these 100 inputs from the first encoder to 50 outputs. The final trained encoder compresses these 50 inputs to 10 outputs. Theoretically, the final 10 outputs contain the geometric and refractive index distribution information of a unit cell. It should be noted that the difference between the input and output of a single encoder cannot be very large or some features of the bitmap will be missing. On the other hand, the amount of the final output should not be very large in order to avoid the noise point produced by superfluous useless information that would reduce the accuracy of prediction. Therefore, the compression process and number of encoders have been optimized to improve the predicted results.

The fitting neural network is illustrated at the bottom of Fig. 1(d). We use the finite element method to calculate the band structure of photonic crystals with various r/a ratios: 0.15, 0.17, 0.19, 0.21, 0.23, 0.25, 0.27, 0.29, 0.31, 0.33, 0.35, 0.37, and 0.39. For each r/a ratio, there are 75 $\vec{k}$ vectors within the irreducible Brillouin zone. For each $\vec{k}$ vector, we calculated five orders of eigen frequencies. Therefore, the training dataset contains 4875 eigen frequencies. Each eigen frequency corresponds to specific r/a ratio, $\vec{k}$ vector, and order of an eigen state. The r/a ratio information is represented by 10 values, which are data compressed from the unit cell bitmap. The $\vec{k}$ vector is represented by one value, that is, the length of the $\vec{k}$ vector within the irreducible Brillouin zone. The order is represented by one integral value between 1 and 5. This means that each eigen frequency corresponds to 12 values in the training dataset. In other words, there are 4875 sets of 12 values and 4875 sets of eigen frequencies in the training dataset. We refer to the 4875 sets of 12 values as input data and the 4875 sets of eigen frequencies as the output target.

We construct two fully connected neural networks as fitting neural networks. The first one includes one hidden layer consisting of 100 neurons. We refer to it as the "one-hidden-layer neural network". The second one has two hidden layers, each consisting of 25 neurons. We refer to it as the "two-hidden-layers neural network". The numbers of neurons in the one-hidden-layer and two-hidden-layers neural networks have been optimized to improve the accuracy of prediction. The neural network toolbox of MATLAB enables us to use the training data to train the above-described fitting neural networks by the backpropagation method. In addition, the trained neural networks can be used to predict the eigen frequency by entering 12 arbitrary values as input data. The training algorithm is Bayesian Regularization.[23] This algorithm is suitable for difficult or noisy datasets. We chose Bayesian Regularization because there are many intersects between photonic bands in the band structure. There are several eigen frequencies close to each other near the intersect points. Only Bayesian Regularization algorithms can handle the eigen frequency prediction well near these points. The training datasets are divided in two parts: training and test parts. 70% of the datasets are used in the training process. The remaining 30% of the datasets are preserved for testing the performance of the trained neural network.

3. Results and Discussion

We plot the photonic crystal band structures calculated by the finite element method and predicted by trained neural networks in Fig. 2. The lattice constant of the photonic crystal is 500 nm. The refractive index of silicon is 3.46. These parameters are frequently used in photonic crystals for the near-IR range. The results calculated by the finite element method and predicted by trained neural networks are denoted by blue circles and red dots, respectively. The r/a ratios in Figs. 2(a) and 2(b) are 0.15, and those in Figs. 2(c) and 2(d) are 0.35. These r/a ratios are included in the training datasets. For the predicted results, the neural network used in the cases of Figs. 2(a) and 2(c) has one hidden layer. The neural network used in the cases of Figs. 2(b) and 2(d) has two hidden layers. In Figs. 2(a) and 2(b), the predicted band structure agrees well with the calculated ones. In Figs. 2(c) and 2(d), the predicted band structure shows agreement with the calculated results in the three bands with the lower frequencies. The discrepancies become obvious at the points marked A, B, A', and B' in Figs. 2(c) and 2(d). The neural networks underestimate the eigen frequencies near these regions. This may be due to the linearity of the photonic band. In Figs. 2(a) and 2(b), the bands in the photonic band structures are more linear and only bend at points X and M in the irreducible Brillouin zone. These behaviors are more easily predicted by the neural network. On the other hand, with r/a = 0.35, the bands in the higher frequency region are curved. More input information may be needed to improve the accuracy of prediction. In addition, comparisons of Figs. 2(a) and 2(c) with Figs. 2(c) and 2(d) indicate that there is no significant intuitive difference between the performance characteristics of one-hidden-layer and two-hidden-layers neural networks.

In the quantitative analysis of the performance characteristics of trained neural networks, the eigen frequencies calculated by the finite element method are referred to as target data and those predicted by the neural network are referred to as output data. In Fig. 3(a), we plot the relationship

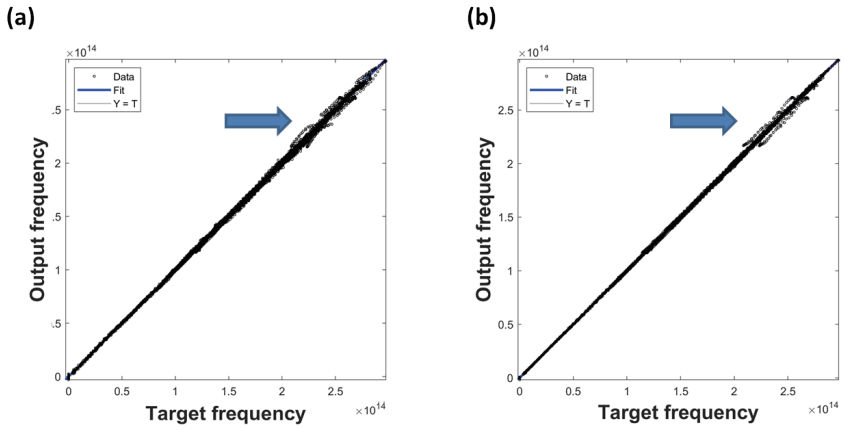

Fig. 3. (Color online) Relationship between target and output frequencies of (a) one-hidden-layer and (b) two-hidden-layers neural networks.

between the target and output data of the one-hidden-layer neural network by black circles. These results include all training datasets. The horizontal axis represents target data and the vertical axis represents output data. If the prediction is 100% correct, all black circles should fall on the line of Output = Target. In Fig. 3(a), most of the black circles are close to the line of Output = Target. The errors between the output and the target in the high-frequency region (marked by a blue arrow) are more significant than those in the low-frequency region. The relationship between the target and output data of the two-hidden-layers neural network is plotted by black circles in Fig. 3(b). The errors between the output and the target in the high-frequency region (marked by a blue arrow) are again higher than those in the low-frequency region. On comparing Fig. 3(a) with Fig. 3(b), the errors of the two-hidden-layers neural network seem smaller than those of the one-hidden-layer neural network. To compare the errors of these two neural networks, we plot the histograms of errors between the target and output frequencies in Fig. 4. Figures 4(a) and 4(b) show the error histograms of the one-hidden-layer and two-hidden-layers neural networks, respectively. The errors represent the frequency difference between the predicted and target results, which are divided into 20 bins in both Figs. 4(a) and 4(b). The *x*-axis shows an error in the order of 10^{12}, which is very small compared with the target frequencies, which are on the order of 10^{14}. The histograms in Fig. 4(b) show that the error distributions are more concentrated near zero error than those in Fig. 4(a). We can conclude that the performance of the two-hidden-layers neural network is better than that of the one-hidden-layer neural network.

To avoid overfitting, we use the proposed neural networks to predict the band structure of photonic crystals with r/a = 0.16. The band structure with r/a = 0.16 is not included in the training dataset. If the predicted band structure agrees well with the results calculated by the finite element method, the neural network is not overtrained. The blue circles in Figs. 5(a) and 5(b) show the band structure with r/a = 0.16, which was calculated by the finite element method. The red dots in Fig. 5(a) represent the band structure predicted by the one-hidden-layer neural network. On the other hand, the red dots in Fig. 5(b) represent the band structure predicted by

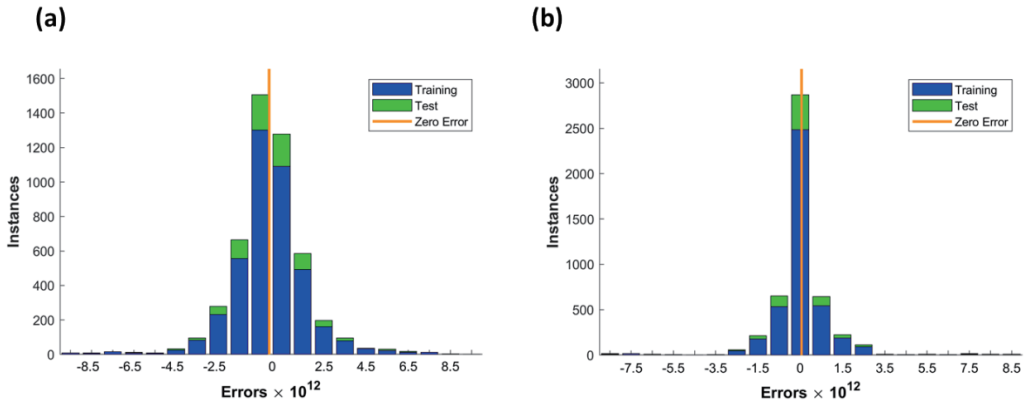

Fig. 4. Error histograms of (a) one-hidden-layer and (b) two-hidden-layers neural networks.

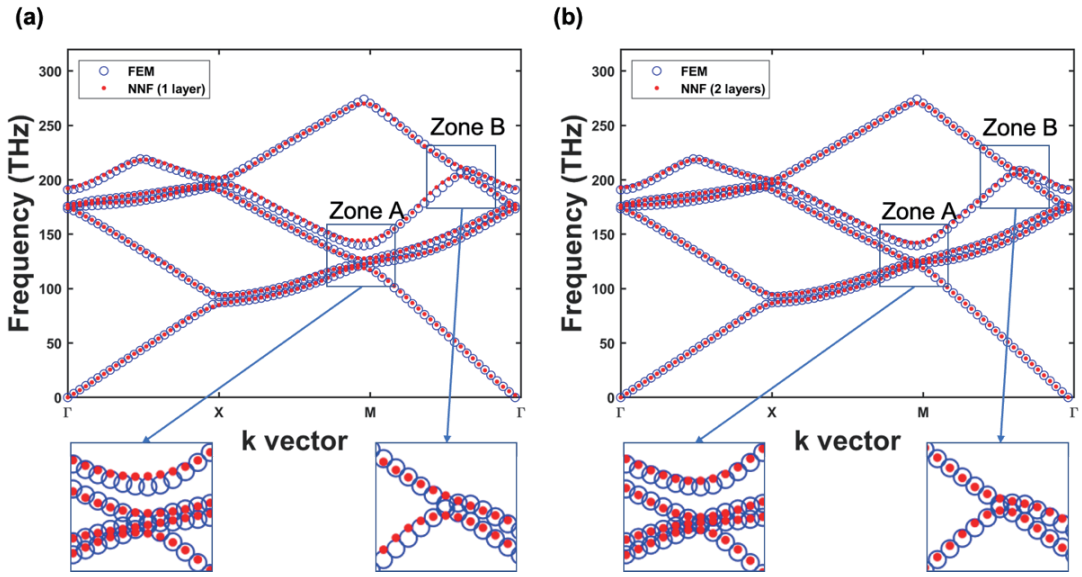

Fig. 5. (Color online) Band structures calculated by finite element method (blue circles) and predicted by trained neural network (red dots). The r/a ratio of the structures in (a) and (b) is 0.16. The numbers of hidden layers of the neural network used are (a) one and (b) two.

the two-hidden-layers neural network. Both predicted results in Figs. 5(a) and 5(b) agree well with the results calculated by the finite element method. Only slight differences can be observed at the bend points of photonic bands. We enlarge Zone A and Zone B in the two band structures and display them at the bottom of Figs. 5(a) and 5(b). The enlarged images show that the two-hidden-layers neural network performs better than the one-hidden-layer neural network. Although the differences are not significant, the important features of a photonic crystal usually appear at the bend points of photonic bands, such as the band gap and Dirac point of the topological photonic crystal. Slow light effects and negative refraction also occur near the bend or reversal points in the band structure. We can conclude that the performance characteristics of

the one-hidden-layer and two-hidden-layers neural networks are similar. However, the two-hidden-layers neural network exhibits a higher accuracy at feature points in the band structure.

4. Conclusions

We proposed a training process to construct artificial neural networks for predicting two-dimensional silicon photonic crystal band structures. The top-view bitmap of the geometric configuration of a unit cell was first compressed by an autoencoder to downgrade the information. We combined the compressed information with the data of wave vectors and eigen orders to form input datasets and used the corresponding eigen frequencies to form output datasets. The input and output datasets were used to train two artificial neural networks: one-hidden-layer and two-hidden-layers neural networks. Both neural networks satisfactorily predicted the band structure of two-dimensional silicon photonic crystals. The predicted band structure agreed well with the results calculated by the finite element method. The two-hidden-layers neural network exhibited better performance at the bend regions of photonic bands.

The autoencoders were generated through unsupervised training. In the previous studies, the exact values of the geometric parameters of devices, such as the r/a ratio of a photonic crystal unit cell and the period and duty cycle of the optical grating were usually directly input to the artificial neural networks. In contrast, in our method, the computer can recognize the unit cell geometric structure automatically instead of requiring the manual input of the parameters. Furthermore, the unsupervised training also resulted in decoders that can reconstruct the geometric configuration of a unit cell from the compressed information from encoders. This implies that we can set the desired photonic crystal band structure and inversely generate the compressed geometric configuration information using the artificial neural network, and then use the decoder to restore this compressed geometric configuration information to form the unit cell of the photonic crystal. This will be very useful for the inverse design of photonic crystals with complex optical properties such as topological photonics or negative refraction.

References

1 E. Yablonovitch: J. Mod. Opt. **41** (1993) 173. https://doi.org/10.1080/09500349414550261
2 S. John: Phys. Rev. Lett. **58** (1987) 2486. https://doi.org/10.1103/PhysRevLett.58.2486
3 T. Baba: Nat. Photon. **2** (2008) 465. https://doi.org/10.1038/nphoton.2008.146
4 Y. Akahane, T. Asano, B. S. Song, and S. Noda: Nature **425** (2003) 944. https://doi.org/10.1038/nature02063
5 M. Gulzari and C. W. Lim: Arch. Comput. Methods Eng. **29** (2022) 1137. https://doi.org/10.1007/s11831-021-09612-8
6 S. Iwamoto, Y. Ota, and Y. Arakawa: Opt. Mater. Express **11** (2021) 319. https://doi.org/10.1364/OME.415128
7 Md. A. Kabir, K. Ahmed, Me. M. Hassan, Md. M. Hossain, and B. Kumar: Opt. Commun. **475** (2020) 126192. https://doi.org/10.1016/j.optcom.2020.126192
8 F. Ghasemi, S. R. Entezar, and S. Razi: Phys. Lett. A **383** (2019) 2551. https://doi.org/10.1016/j.physleta.2019.05.016
9 J. Hou, M. Li, and Y. Song: Nano Today **22** (2018) 132. https://doi.org/10.1016/j.nantod.2018.08.008
10 L. Ferrier, H. S. Nguyen, C. Jamois, L. Berguiga, C. Symonds, J. Bellessa, and T. Benyattou: APL Photonics **4** (2019) 106101. https://doi.org/10.1063/1.5104334
11 D. Headland, W. Withayachumnankul, R. Yamada, M. Fujita, and T. Nagatsuma: APL Photonics **3** (2018) 126105. https://doi.org/10.1063/1.5060631
12 Z. Xiong, W. Chen, Z, Wang, J, Xu, and Y. Chen: Front. Optoelectron. **14** (2021) 148. https://doi.org/10.1007/s12200-021-1213-5

13 F. Segovia-Chaves and H. Vinck-Posada: Phys. B: Condens. Matter **545** (2018) 203. https://doi.org/10.1016/j.physb.2018.06.014
14 K. H. Jin, M. T. McCann, E. Froustey, and M. Unser: IEEE Trans. Image Process **26** (2017) 4509. https://doi.org/10.1109/TIP.2017.2713099
15 F. Barreto, J. Sarvaiya, and S. Patnaik: Adv. Technol. Innov. **7** (2022) 279. https://doi.org/10.46604/aiti.2022.8308
16 C.-C. Ho, E. Su, P.-C. Li, M. J. Bolger, and H.-N. Pan: Adv. Technol. Innov. **5** (2020) 76. https://doi.org/10.46604/aiti.2020.4278
17 D. Lee, S.-J. Lee, and Yu-Jeong Seo: Int. J. Eng. Technol. Innov. **10** (2020) 75. https://doi.org/10.46604/IJETI.2020.4354
18 X, Li, S. Xu, and X. Hua: Symmetry **13** (2021) 87. https://doi.org/10.3390/sym13010087
19 B. Duan, H. Zou, J. Chen, C. H. Ma, X, Zhao, X. Zhen, G. Wang, L. Liu, and D. Yang: Photonics Res. **10** (2022) 2343. https://doi.org/10.1364/PRJ.464133
20 T. Asano and S. Noda: Opt. Express **26** (2018) 32704. https://doi.org/10.1364/OE.26.032704
21 R. Singh, Anu Agarwal, and B. Anthony: Opt. Express **28** (2020) 27893. https://doi.org/10.1364/OE.398926
22 C. Kittel: Introduction to Solid State Physics (John Wiley & Sons, Inc, USA, 2004) Chap. 2.
23 D. J. C. MacKay: Neural Comput. **4** (1992) 415. https://doi.org/10.1162/neco.1992.4.5.720

About the Authors

Wei-Shan Chang received her B.S. and M.S. degrees from Chung Shan Medical University, Taiwan, in 2008 and 2010, respectively. She is currently a Ph.D. student in the Institute of Photonics, National Changhua University of Education. Her research interests are in photonic and phononic crystals.

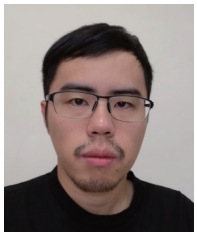

Ying-Pin Tsai received his BS degree from the Department of Physics of National Changhua University of Education, Taiwan, in 2014 and his MS degree from the Graduate Institute of Photonics, National Changhua University of Education, Taiwan, in 2017. Currently, he is a Ph.D candidate in the College of Photonics, National Yang Ming Chiao Tung University, Tainan City, Taiwan. He has been a researcher of metamaterials at National Yang Ming Chiao Tung University since 2018. His current research interests include photonic crystals, phononic crystals, acousto-optics structures, and ultrasound structures.

Chi-Tsung Chiang received his MS degree from National Changhua University of Education (NCUE), Taiwan, in 2013. Currently, he is a Ph.D candidate in the College of Photonics, National Changhua University of Education, Taiwan. He has been a researcher of metamaterials at NCUE since 2017. His current research interests include photonic crystals, phononic crystals, acousto-optics structures, and ultrasound structures.

Fu-Li Hsiao received his B.S. degree from National Changhua University of Education, Taiwan, in 2002 and his Ph.D. degrees from the National Central University, Taiwan, and University of Franche-Comté, France, in 2008. Since 2010, he has been a professor at the Institute of Photonics, National Changhua University of Education, Taiwan. His research interests are in photonic crystals, phononic crystals, optomechanics, and metamaterials.